





Article

Simultaneous Removal of As(III) and Fluoride Ions from Water Using Manganese Oxide Supported on Graphene Nanostructures (GO-MnO₂)

Athanasia K. Tolkou ^{1,2,*}, Dimitrios G. Trikkaliotis ², George Z. Kyzas ², Ioannis A. Katsoyiannis ¹
and Eleni A. Deliyanni ¹

¹ Laboratory of Chemical and Environmental Technology, Department of Chemistry, Aristotle University of Thessaloniki, 54124 Thessaloniki, Greece

² Department of Chemistry, International Hellenic University, 65404 Kavala, Greece

* Correspondence: tolkatha@chem.ihu.gr; Tel.: +30-25-1046-2218

Abstract: In the present research, the use of manganese oxides supported on graphene nanostructures (GO-MnO₂), which support the synergistic action of adsorption and oxidation, in the combined removal of arsenic and fluoride from drinking water was studied. The simultaneous occurrence of fluoride and arsenic in groundwater is one of the major environmental problems, occurring mainly in anhydrous regions of Latin America and the world. These pollutants cause significant health problems and are difficult to remove simultaneously from drinking water. The structure of GO-MnO₂ was characterized by the application of FTIR, EDS and SEM techniques. The effects of the adsorbent's dosage, the pH value, the contact time and the initial concentrations of As(III) and F ions (F⁻) were examined with respect to the removal of As(III) and F ions. According to the results, the presence of arsenic enhances fluoride removal with increasing arsenic concentrations, and the presence of fluoride enhances arsenic removal with increasing fluoride concentrations, mainly at a neutral pH value. The co-presence removal efficiencies were 89% (a residual concentration of 1.04 mg/L) for fluoride and about 97% (a residual concentration of 2.89 µg/L) for arsenic.

Keywords: arsenic; fluoride; adsorption; graphene; manganese oxides



Citation: Tolkou, A.K.; Trikkaliotis, D.G.; Kyzas, G.Z.; Katsoyiannis, I.A.; Deliyanni, E.A. Simultaneous Removal of As(III) and Fluoride Ions from Water Using Manganese Oxide Supported on Graphene Nanostructures (GO-MnO₂).

Sustainability **2023**, *15*, 1179. <https://doi.org/10.3390/su15021179>

Academic Editor: Luca Di Palma

Received: 6 December 2022

Revised: 30 December 2022

Accepted: 5 January 2023

Published: 8 January 2023



Copyright: © 2023 by the authors. Licensee MDPI, Basel, Switzerland. This article is an open access article distributed under the terms and conditions of the Creative Commons Attribution (CC BY) license (<https://creativecommons.org/licenses/by/4.0/>).

1. Introduction

Arsenic (As) and fluoride (F) are globally recognized as two of the most serious inorganic pollutants in drinking water, and their co-existence in groundwater has become one of the most significant environmental issues worldwide due to their toxic effects both on living beings and on the ecological environment [1]. According to the World Health Organization (WHO), the maximum permissible limit of As in drinking water is 0.010 mg/L (10 µg/L), and that of F is 0.6–1.5 mg/L [2]. Extended consumption of arsenic-containing waters leads to several health effects, such as cancers of the skin, lungs and bladder [3], diabetes and infant mortality [4]. In the case of fluoride, even though a low intake of fluoride is essential for skeleton and dental health, an excess intake leads to dental and skeleton fluorosis [5]. Hence, the combined exposure to As and F may lead to both endemic fluorosis and arsenicosis, while studies showed a reduction of IQ levels and mental functioning in children [6].

Arsenic in natural waters, depending on the existing oxidation–reduction conditions and pH values [7], is mostly found as As(III) (H₃AsO₃) and/or As(V) (H₃AsO₄, H₂AsO₄⁻ and HAsO₃²⁻) [8,9], while the As(III) oxidation state is more toxic in relation to the compounds of As(V) [10]. Moreover, fluoride is presented as fluorine, which is an active non-metal element that has a negatively charged species, i.e., F ions.

The risks and health effects of exposure to each individual pollutant are well documented [1]. However, there are only a few references for the risk of simultaneous exposure

to both As and F. Concentrations of arsenic and fluoride above the WHO drinking water standard limits have been detected in Argentina, China, Mexico, Bangladesh, Vietnam, Pakistan and Cambodia [11], etc. Specifically, in Argentina's groundwater samples, high levels of As and F, i.e., 250 µg/L and 12 mg/L, respectively, were found, while in Pakistan's groundwater the relative concentrations were found to be as high as 2400 µg/L for As and 22.8 mg/L for F [12,13].

Various technologies have been developed for the removal of As and F in order to achieve these permissible limits [14–18], and among them, adsorption with modified activated carbons [19,20] is a very promising and widely applied technique [21,22]. However, several studies [12,17,23] have been carried out to investigate the simultaneous removal of arsenic and fluoride, and a reduction in the removal efficiency of one of the two pollutants is generally observed. The removal technologies [24] that have been used to remove these two pollutants simultaneously are coagulation [12], adsorption [12,25], membrane filtration [26] and electrocoagulation [13,27,28]. Among these, adsorption is regarded as one of the most promising and economical techniques, and several materials [15,29] can be applied that have great potential to remove both pollutants simultaneously [30]. Specifically, modified yak dung biochar [31], hydrated cement, bricks and marble powder [23] and granular TiO₂-La [32] are some of the adsorbents used in the literature for simultaneous arsenic and fluoride removal. Coagulation is another economical conventional technology that has been used [12], but, in this study, only adsorption was selected for further evaluation.

In this study, manganese oxide supported on graphene nanostructures (GO-MnO₂) was tested for the simultaneous removal of As(III) and F ions. The idea for this application arose from previous studies found in the literature, as graphene nanosheets and graphene composites have been used for the removal of metal ions [33,34]. In addition, enhanced As(V) and As(III) removal from groundwater was observed using iron oxide and manganese oxide pillared clays [35,36]. Generally, manganese oxide is not used directly because it may be required in high quantities [37]. Recent studies have proved that MnO₂ particles have a large surface area [38], and, therefore, several modified manganese oxide based materials have been used for the efficient removal of heavy metals, such as Pb(II), Cd(II), Ni(II) Zn(II) and Cu(II), from aqueous systems [39–43]. Moreover, Luo et al. [44] described the use of GO as a substrate to support zirconium hydroxide (ZrO(OH)₂) nanoparticles for the simultaneous removal of As(III) and As(V) from aqueous solutions. Additionally, Luo et al. [45], in their study, combined the oxidizing ability of manganese dioxide, the large surface area of GO and the magnetic characteristics of Fe₃O₄, aiming at synthesizing a new adsorbent (Fe₃O₄-RGO-MnO₂) for As removal. On the other hand, GO/Al₂O₃, produced by GO and γ-Al₂O₃ [46], Graphene Oxide–Aluminum Oxyhydroxide (GO–Al–O(OH)) [47], Graphene Oxide Anchored Sand (ZIGCS) functionalized by Zr(IV) [48] and Graphene Oxide/Eggshell (GO/ES) [49] are some of the adsorbents based on graphene oxide and have been used in the literature for the removal of fluoride from water [15]. Manganese oxides, such as manganese modified activated alumina, MAA [50], bentonite-smectite rich clay [50] and manganese dioxide with dispersion over disposed earthenware (DEW) [37], were also tested for fluoride removal.

GO-MnO₂ is an adsorbent that the authors have used successfully in their previous studies for effective dye degradation [51]. In addition, GO-MnO₂ nanocomposites are easier to separate from water, and their high conductivity can enhance electron transfer [51,52]. Considering the advantages of graphene, e.g., its large specific surface area and abundance in oxygen functional groups [53,54], and of manganese oxides, which exhibited a large specific surface area that can provide the reaction with additional active sites [50], this study involves testing the effectiveness of this material in the combined removal of arsenic and fluoride from water. The effect of the pH value, the initial concentration of As(III) and F ions and the dose of the adsorbent dose were investigated, while the structure and the morphology of GO-MnO₂ were analyzed using EDS, FTIR and SEM. Additionally, kinetic and isotherm models were also applied to evaluate the adsorption process, and experiments with GO and MnO₂ took place separately for comparison reasons.

2. Materials and Methods

2.1. Materials

All reagents used were of an analytical grade. A sodium fluoride (NaF) solution (Merck) was used for the preparation of simulated fluoride water. A 1000 mg F⁻/L stock solution was prepared by dissolving 2.210 g of NaF in 1000 mL of deionized water. Then, the required concentrations of fluoride ions were obtained by diluting the stock solution. An As(III) stock solution (100 mg As(III)/L) was prepared by dissolving 0.1733 g of sodium metarsenite (AsNaO₂) (Merck) in 1000 mL of deionized water and stored in 4 °C for further use in the experiments. The pH was appropriately adjusted using 0.01–0.1 M of NaOH ACS reagent, ≥97.0%, pellets (Sigma-Aldrich) or 0.01–0.1 M of HCl 37% (Panreac).

2.2. Synthesis of GO, MnO₂ and GO-MnO₂

The GO, MnO₂ and GO-MnO₂ were previously synthesized and used in other studies by the authors [51,55]. Very briefly, the GO was prepared by using the modified Hummer's method [56], as improved by Debnath et al. (2014) [57]. For the preparation of the manganese oxide (MnO₂), a 30 mL solution of KMnO₄ (0.21 mol/L) was added dropwise to a solution of MnSO₄ (0.2 mol/L) under stirring, and then MnO₂ was formed. A GO-MnO₂ composite resulted after the ultra-sonication for 1 h of a solution prepared by adding 2 g of graphite oxide in 175 mL of deionized water. Then, an appropriate amount of KMnO₄ solution (0.8 g in 100 mL of deionized water) was slowly added under vigorous stirring and kept in darkness for 12 h, and the resulting GO-MnO₂ was collected by centrifugation, washed with deionized water and absolute ethanol and freeze-dried. According to Saroyan et al. [51], the successful oxidation of graphite into graphite oxide was confirmed by a relative peak at XRD patterns.

2.3. Analytical Determinations

For the determination of the F ions' residual concentration, the application of the SPADNS photometric method [58] was used, which is based on the reaction between fluoride ions and Zirconium, splitting a part of it into a colorless complex anion (ZrF₆₂₋) and the dye. As the amount of fluoride increases, the color produced becomes progressively lighter, compared to a standard fluoride solution. An amount of 2 mL of a mixed solution of Zr-SPADNS complex, with a long resistance to time in the dark, previously synthesized [59], was added to 10 mL of (diluted) samples and mixed well. The absorbance at 570 nm was determined with the UV-Vis (WTW Spectroflex 6100) spectrophotometer for the calculation of the residual concentration of fluoride ions via a standard curve. The arsenic concentration was measured by atomic absorption spectroscopy coupled with a graphite furnace (Varian Zeeman AA240Z with GTA 120; Hansen Way, Palo Alto, CA, USA), which has a detection limit of 1 µg/L.

2.4. Characterization Techniques

The surface morphology of the GO, MnO₂ and GO-MnO₂ before and after adsorption was observed using Scanning Electron Microscopy (SEM) (Jeol JSM-6390 LV, JEOL Ltd, Akishima, Tokyo, Japan) scanning electron microscope: equipped with an energy dispersive X-ray system (EDS) for surface element analysis. The surface chemical bonds and functional groups were analyzed by Fourier Transform Infrared Spectroscopy (FT-IR, Perkin Elmer, New York, NY, USA), in the range of 4000–400 cm⁻¹.

2.5. Adsorption Experiments

Adsorption experiments were carried out by introducing a quantity of adsorbent into 15 mL falcon tubes (10 mL is the volume of solution) containing arsenic, fluoride or a mixture of both arsenic and fluoride solution at indicated initial concentrations and at a constant temperature. The mixture was agitated using a Trayster overhead shaker and a Loopster rotator at a constant stirring speed (80 rpm). A number of experimental variables such as pH (3.0–9.0 ± 0.1), the initial concentration of F ions (2–100 mg/L), the

initial As(III) concentration (25–500 µg/L), the adsorbent dose (0.5–2.0 g/L) and the contact time (10–360 min for kinetics and 24 h for equilibrium) were independently varied by keeping other parameters constant during the experiments. The initial As(III) and F ions concentrations selected for consideration are the relevant environmental concentrations representing the contaminated waters. After adsorption, the water samples collected were filtered through a 0.45 µm pore size nylon filter and several parameters were determined in the filtrate. The results are the mean of three replicate experiments. The percentage removal (%R) of F⁻ and As(III) was determined from the following Equation (1):

$$R (\%) = \left(\frac{C_0 - C_f}{C_0} \right) \times 100\% \quad (1)$$

where C_0 is the initial F⁻ concentration (mg/L) or As(III) concentration (µg/L), and C_f is the final F ions concentration (mg/L) or As(III) concentration (µg/L) after treatment.

The adsorption capacity of the adsorbents (Q_e) (mg/g for F ions and µg/g for As(III)) was calculated from the following Equation (2):

$$Q_e = \frac{(C_0 - C_e) \times V}{m} \quad (2)$$

where C_e is the F⁻ concentration (mg/L) or As(III) concentration (µg/L) at equilibrium, V (L) is the volume of the solution and m (g) is the mass of the adsorbent used.

2.5.1. Equilibrium Experiments

For the isothermal experiments, a fixed amount of adsorbent sample (g) was added to 10 mL of As(III) solution (25–500 µg/L) in the presence of F ions (10 mg/L) or to 10 mL of F ions solution (2–100 mg/L) in the presence of As(III) (100 µg/L) in 15 mL falcon tubes. The adsorption experimental results were fitted to the Langmuir and Freundlich isotherm models.

The Langmuir model correlates the solid phase adsorbate concentration (Q_e) and the uptakes to the equilibrium liquid concentration and is expressed as Equation (3):

$$Q_e = \frac{Q_m K_L C_e}{1 + K_L C_e} \quad (3)$$

where Q_m is the theoretical monolayer/maximum adsorption capacity (mg/g for F ions and µg/L for As(III)), and K_L is related to the energy of As(III) (L/µg) or F ions (L/mg) adsorption.

The Langmuir theory assumes that the adsorbent has a limited adsorption capacity (Q_m), while the adsorbate forms a monolayer on the adsorbent surface, and that there is a lack of interface between the adsorbed molecules [60].

The Freundlich model [61] outlines the interrelation between the F ions or As(III) equilibrium concentrations (mg/L for F ions and µg/L for As(III)) and the uptake capacities, Q_e (mg/g for F ions and µg/g for As(III)), of the adsorbent and is expressed as Equation (4):

$$Q_e = K_F C_e^{1/n} \quad (4)$$

where K_F is a constant related to adsorption capacity while $1/n$ is a constant related to the intensity of adsorption or the surface heterogeneity; $1/n = 0$ is for the heterogeneous phase; $1/n < 1$ is for a normal Freundlich isotherm; and $1/n > 1$ indicates a cooperative adsorption.

2.5.2. Kinetics Experiments

Two widely used models, i.e., the pseudo-first-order (PFO) and pseudo-second-order (PSO) kinetics models, were investigated to fit the kinetics of F⁻ or As(III) adsorption. The calculated adsorption kinetic parameters were further analyzed to estimate the adsorption

rates as well as to determine the potential reaction mechanism. The pseudo-first-order model used for the data analysis is as shown below as Equation (5):

$$Q_t = Q_e(1 - e^{-k_1 t}) \quad (5)$$

where Q_e is the amount of F ions or As(III) adsorbed at equilibrium (mg/g for F ions and $\mu\text{g/g}$ for As(III)), Q_t is the amount of F ions or As(III) adsorbed at time t (mg/g for F ions and $\mu\text{g/g}$ for As(III)), k_1 is the rate constant of the PFO model (1/min) and t is the time (min).

The pseudo-second-order model used for the data analysis is as shown below as Equation (6):

$$Q_t = \frac{k_2 Q_e^2 t}{1 + k_2 Q_e t} \quad (6)$$

where Q_e is the amount of F^- or As(III) adsorbed at equilibrium (mg/g for F ions and $\mu\text{g/g}$ for As(III)), Q_t is the amount of F ions or As(III) adsorbed at time t (mg/g for F ions and $\mu\text{g/g}$ for As(III)), k_2 is the rate constant of the PSO ($\text{g}/(\text{mg min})$ for F ions and $\text{g}/(\mu\text{g min})$ for As(III)) and t is the time (min).

3. Results and Discussion

3.1. Characterization

3.1.1. Scanning Electron Microscopy (SEM)

Figure 1 presents the SEM images of all of the adsorbents (GO, MnO_2 and GO- MnO_2), before (Figure 1a–c) and after the adsorption of As(III) (Figure 1d–f), F ions (Figure 1g–i) and the simultaneous presence of the two anions (Figure 1j–l). As shown, GO is formed in large sheet-like layers with a typical smooth surface and some wrinkles [62] (Figure 1a) which seem to be filled during the adsorption of ions, and, especially in the case of the simultaneous adsorption of As(III) and F ions (Figure 1j), the surface appears to be smoother and more saturated. In addition, the SEM images of MnO_2 (Figure 1b,e,h,k) show a high monodispersed flower-like nanostructure [63] that does not appear to be significantly modified upon anion adsorption. Moreover, the SEM images of the GO- MnO_2 nanocomposite (Figure 1c) revealed a partially layered structure, which was indicative of the partial exfoliation of GO in the composite [51], which is enhanced upon the adsorption of As(III) and fluoride ions (Figure 1l).

The SEM-EDS analysis of all of the adsorbents applied in this study, i.e., GO, MnO_2 and GO- MnO_2 , before and after the adsorption of As(III), F^- and the two anions simultaneously are presented in Table 1. According to the % (w/w) values of the GO- MnO_2 EDS analysis, the evident elements were manganese, carbon and oxygen, with the carbon originating from the GO, the oxygen from the GO and the MnO_2 and the manganese from the MnO_2 . In addition, F and As were detected on the surface of all the three adsorbents, confirming that the relative adsorption had occurred. Furthermore, the SEM-elemental maps of the adsorbed As(III) and F ions to the GO- MnO_2 (inset: mapping from Figure 1l) are shown in Figure 2. As depicted, the uniform distribution of As(III) and F ions on the surface of the GO- MnO_2 adsorbent is confirmed.

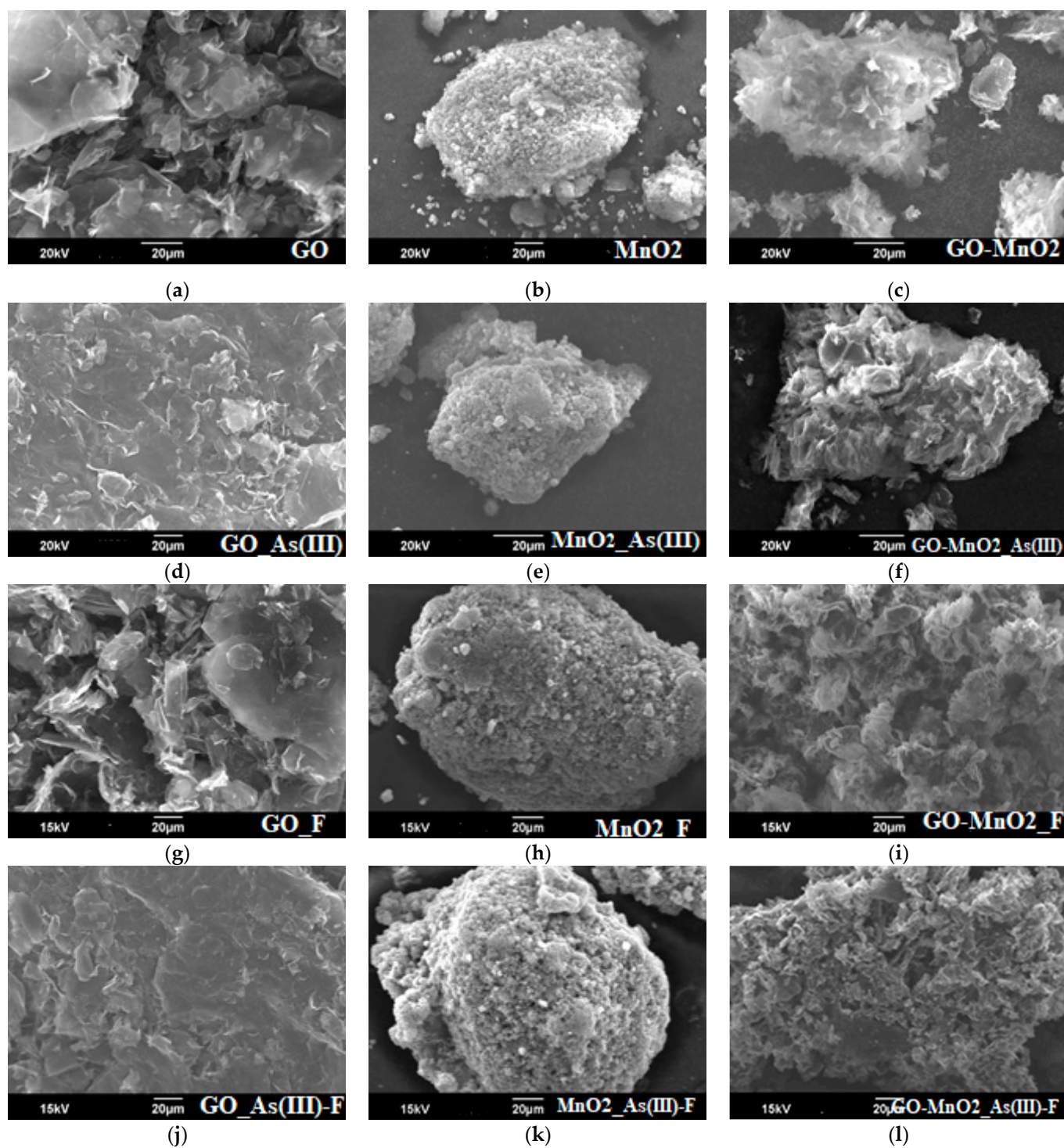
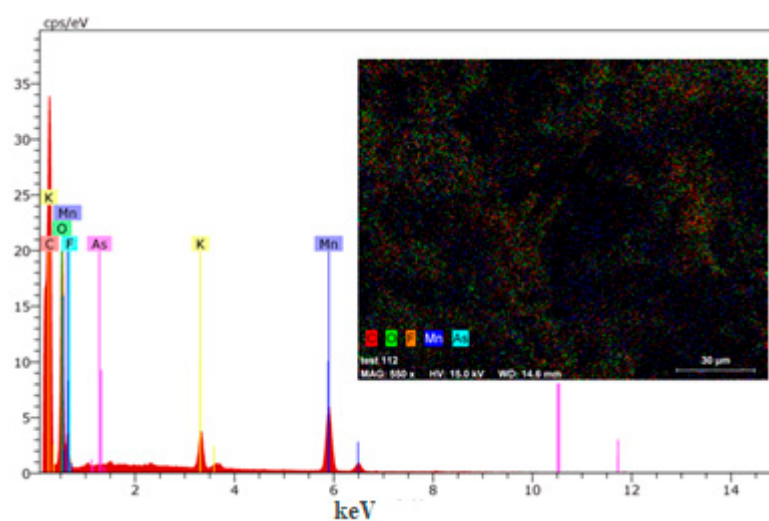


Figure 1. The SEM images of the adsorbents before and after adsorption of As(III), F^- , and the simultaneous addition of As(III) and F^- ions. (a) GO; (b) MnO₂; (c) GO-MnO₂ before the adsorption. (d) GO; (e) MnO₂; (f) GO-MnO₂ after the adsorption of As(III). (g) GO; (h) MnO₂; (i) GO-MnO₂ after the adsorption of fluoride ions. (j) GO; (k) MnO₂; (l) GO-MnO₂ after the simultaneous adsorption of As(III) and fluoride ions.

Table 1. Elemental composition by SEM/EDS analysis of adsorbents before and after adsorption.

% (w/w)	GO	MnO ₂	GO-MnO ₂
Carbon	43.84	-	28.70
Sulfur	14.56	-	-
Oxygen	41.6	68.91	64.81
Manganese	-	27.86	3.93
Potassium	-	2.63	2.56
Chlorine	-	0.60	-
% (w/w)	GO_As(III)	MnO ₂ _As(III)	GO-MnO ₂ _As(III)
Arsenic	0.10	1.19	0.56
Carbon	75.93	-	26.89
Sulfur	0.57	-	-
Oxygen	23.39	58.77	63.38
Manganese	-	36.35	6.52
Potassium	-	3.68	2.64
% (w/w)	GO_F ⁻	MnO ₂ _F ⁻	GO-MnO ₂ _F ⁻
Carbon	73.65	-	22.22
Fluorine	2.22	13.63	4.48
Sulfur	0.51	-	-
Oxygen	23.61	59.54	50.31
Manganese	-	24.74	19.61
Potassium	-	2.09	3.39
% (w/w)	GO_As(III)-F ⁻	MnO ₂ _As(III)-F ⁻	GO-MnO ₂ _As(III)-F ⁻
Carbon	73.21	-	22.07
Arsenic	0.07	2.01	4.24
Fluorine	1.78	0.51	8.38
Sulfur	0.36	-	-
Silicon	0.24	-	-
Oxygen	24.34	29.04	50.39
Manganese	-	63.05	12.31
Potassium	-	5.39	2.61

**Figure 2.** Elemental analysis of the adsorbed As(III) and F ions to GO-MnO₂.

3.1.2. Fourier Transform Infrared Spectroscopy (FTIR) Analysis

As illustrated in Figure 3, the synthesized GO-MnO₂ has all the typical bands of GO [62]. The binding of MnO₂ to GO shifts the C=C peak to a higher energy (1620–1577 cm⁻¹), decreases the carbonyl volume (1710 cm⁻¹), and broadens the epoxy and alkoxy bands at 1171 cm⁻¹ and 1044 cm⁻¹, respectively. In the spectrum of the adsorbed F⁻ to GO-MnO₂ a shift in the band of carboxyls to higher energy (~20 cm⁻¹) was observed, along with the elimination of the epoxy stretching groups at 1288 cm⁻¹, while the spectrum of the adsorbed As(III) to GO-MnO₂ shows the shifting of both the carboxyl and alkoxy bands to higher energy (~10 cm⁻¹). When studying the spectrum of the simultaneous adsorption of As(III) and F ions to GO-MnO₂, the abovementioned changes can be still observed; thus, it can be stated that the carboxyl groups bind both As(III) and F⁻ ions, the epoxy groups bind the F⁻ ions and the alkoxy groups bind the As(III) ions.

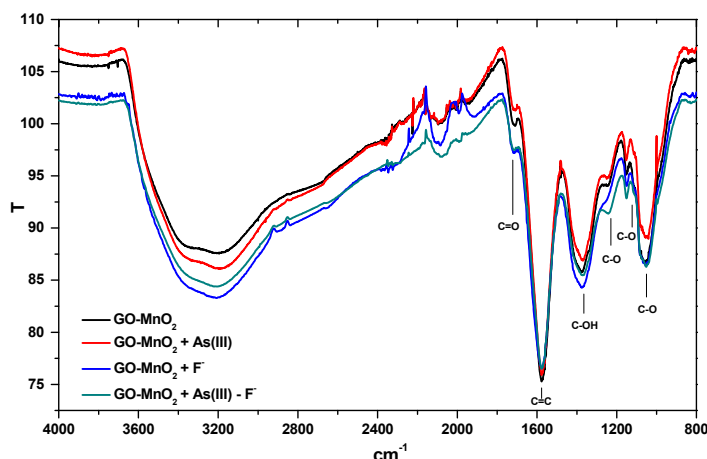


Figure 3. FTIR spectra of GOMnO₂ with the bonded As(III) and F⁻ ions.

3.2. Batch Adsorption Experiments

3.2.1. Effect of Adsorbent Dose and Comparison of Adsorbents

The effect of the adsorbent’s dosage, in parallel with the effect of the type of the adsorbent (GO, MnO₂ and GO-MnO₂) in three different pH values, was studied in order to determine the feasibility of the adsorbents in simultaneous As(III) and F⁻ removal through batch experiments. Hence, Figures 4 and 5 show this effect in detail on the As(III) percentage removal in absence and presence of F ions and on the F ions percentage removal in absence and presence of As(III) at different pH values, i.e., pH 4.0 ± 0.1; pH 7.0 ± 0.1 and pH 9.0 ± 0.1. The initial As(III) concentration was 100 µg/L, the initial F ions concentration was 10 mg/L, and several doses of the adsorbent were applied at room temperature (298 K).

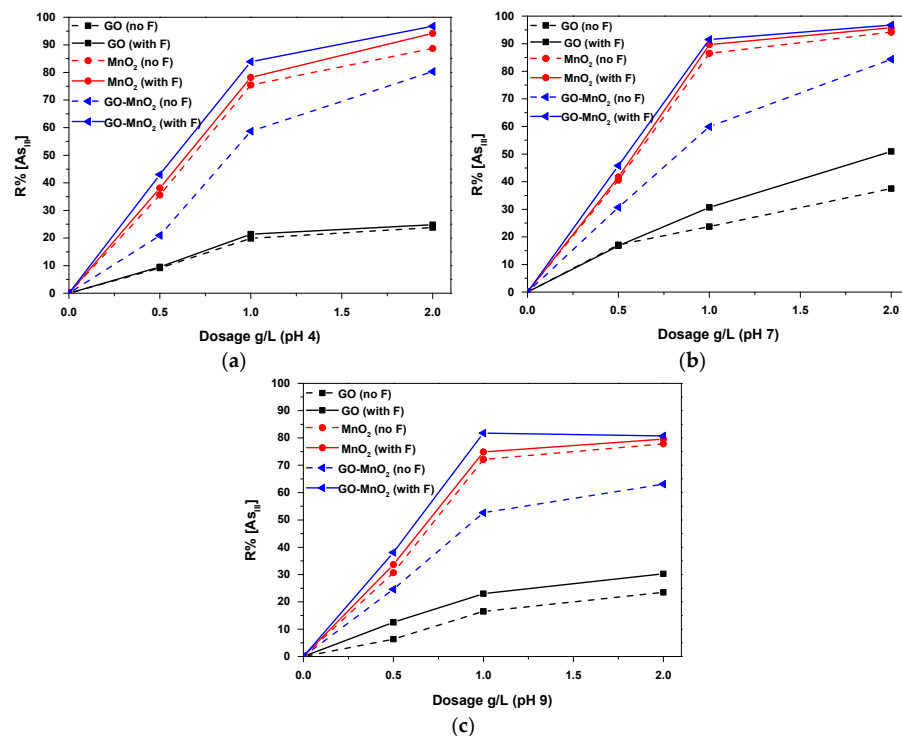


Figure 4. Comparison and effect of adsorbent dose on As(III) R% removal in absence and presence of F ions at different pH values: (a) pH 4 ± 0.1; (b) pH 7 ± 0.1 and (c) pH 9 ± 0.1; initial As(III) concentration 100 µg/L; initial F ions concentration 10 mg/L, T = 298 K, contact time 24 h, in deionized water.

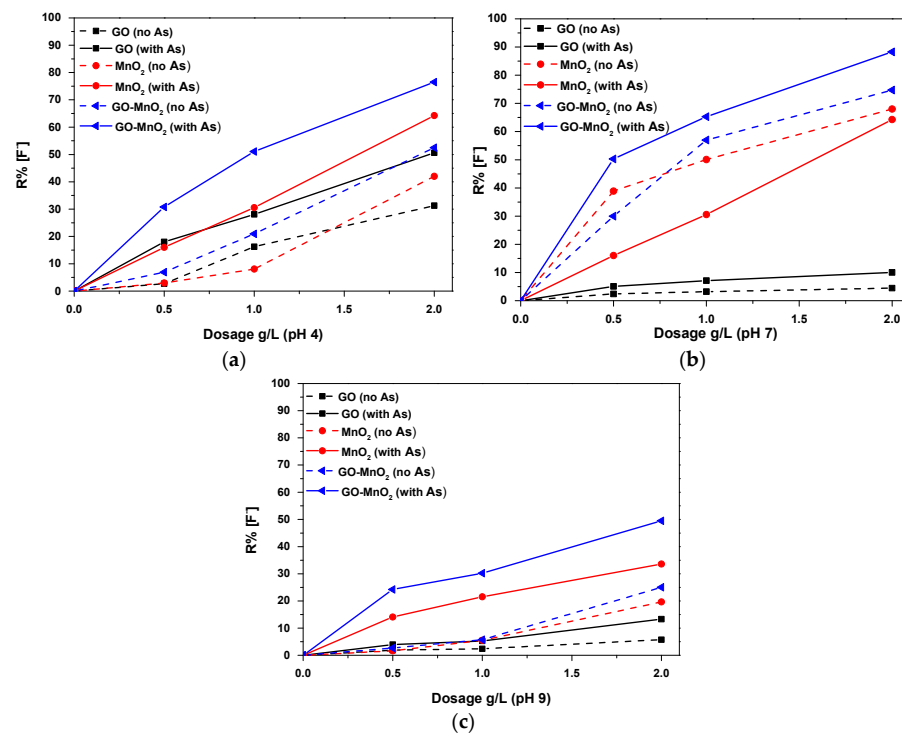


Figure 5. Comparison and effect of adsorbent dose on F ions R% removal in absence and presence of As(III) at different pH values: (a) pH 4.0 ± 0.1 ; (b) pH 7.0 ± 0.1 and (c) pH 9.0 ± 0.1 ; initial As(III) concentration $100 \mu\text{g/L}$; initial F ions concentration 10 mg/L , $T = 298 \text{ K}$, contact time 24 h , in deionized water.

Initially, as depicted in Figure 4, regarding the removal of As(III), GO is by far the least effective adsorbent at all applied pH values and doses, whether in the presence or absence of fluoride ions. On the other hand, MnO₂ is already known as an adsorbent for the effective removal of As(III) through oxidation [64], and this was also confirmed by the experiments in this research. Furthermore, as it appears, its effectiveness is not affected by the presence of F ions.

However, the greatest variation is observed when GO-MnO₂ is used as the adsorbent, and, comparatively, its effectiveness in removing As(III) increases significantly in the simultaneous presence of F ions, at all applied pH values. In particular, at pH 7 (Figure 4b), with a dose of 1 g/L , a removal of $>90\%$ is achieved, and, with 2 g/L , it reaches 98% (compared to 51 and 95% for and respectively). The corresponding percentage removal (Figure 4b) of As(III) in the absence of F ions at pH 7 with 2 g/L of GO-MnO₂ is only 84% . Therefore, from this series of experiments, it follows that the removal of F ions in the presence or absence of As(III) must be studied accordingly in order to be able to draw a conclusion about the possible mechanism.

Observing the diagrams in Figure 5, regarding F ions % removal, GO is not even in this case effective at almost all pH values (with an exception at pH 4 (Figure 5a), where it is slightly better), whether in the presence or absence of As(III). Moreover, contrary to the case of arsenic (Figure 4), MnO₂ is also not efficient in the removal of fluoride ions, and, in fact, at pH 7 (Figure 5b), the efficiency decreases when As(III) is also present, obviously due to the high selectivity of MnO₂ at As(III), which binds to active sites on the MnO₂ surface for its oxidation.

Finally, the maximum removal of fluoride ions is achieved, according to the results in the diagrams in Figure 5, with the application of GO-MnO₂ as the adsorbent. In particular, at pH 7 with a dose of 2 g/L , a removal of almost 90% is achieved with the simultaneous presence of arsenic in the solution, thus maintaining the residual concentration of F ions within the desired limits (i.e., 1 mg/L). It should be noted that the specific conditions are also effective in the case of As(III) in the presence of fluoride ions, as mentioned above in

Figure 4; therefore, the dose of 2 g/L is optimally chosen for the subsequent experiments evaluating the adsorption. For comparison reasons, the application of MnO₂ will be studied at the same time.

3.2.2. Effect of Initial pH Solution

The effect of pH on the removal of As(III) and F ions was studied at different pH values of the solution ranging from 3.0 ± 0.1 to 9.0 ± 0.1 (contact time 24 h; temperature 298 K, dosage 2 g/L), as illustrated in Figure 6. As shown in Figure 6a, the removal of As(III) in the presence of fluoride anions is favored at low to neutral pH values (mildly acidic conditions) with a maximum percentage removal exhibited at pH 7 (98%) on GO-MnO₂. For F ions removal (Figure 6b) in the presence of As(III) anions, especially with the adsorption on GO-MnO₂, the maximum percentage removal was achieved at neutral pH value (88%). Further increment of the pH, for both anions, progressively resulted in a reduced adsorbent capacity of the GO-MnO₂, and at pH 9 there was a sharp decrease of the percentage removal, i.e., 80% and 44% for As(III) and F ions, respectively.

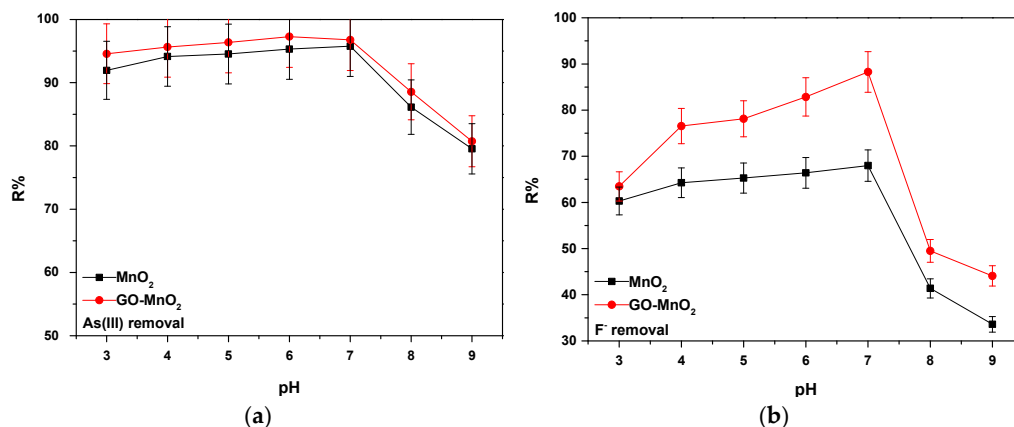


Figure 6. Effect of initial solution pH on the adsorption of (a) As(III) in the presence of F ions, (b) F ions in the presence of As(III), in terms of R% removal; initial As(III) concentration 100 µg/L; initial F ions concentration 10 mg/L, pH 3.0–9.0 ± 0.1, dosage 2 g/L, T = 298 K, contact time 24 h, in deionized water.

In order to better understand the effect of pH, the p*H*_{pzc} measurements of the adsorbent were conducted in the range of 2.0–10.0 ± 0.1, as p*H*_{pzc} is the critical point from which the surface charge of the adsorbent converts from positive to negative, with a possible impact to the interface between the adsorbate and the adsorbent. p*H*_{pzc} was calculated by the relative curve plotted against Δp*H* vs p*H*_{initial}, using pH drift method. As illustrated in Figure 7 the relative p*H*_{pzc} value was found to be 5.04 for GO-MnO₂.

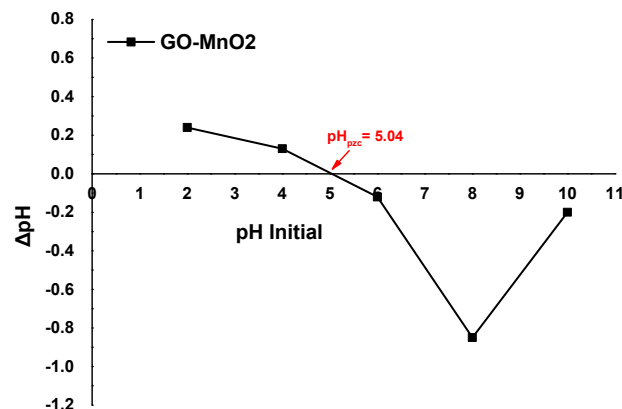


Figure 7. Determination of p*H*_{pzc} of GO-MnO₂ using pH drift method.

Based on the results of this study, providing an efficient pH value of 7.0 ± 0.1 for the simultaneous removal of As(III) and F ions, compared with the relative pH_{ZPC} value equal to 5.04 for GO-MnO₂, it can be assumed that, at pH above 5.04, the predominant surface area of GO-MnO₂ is negative, which is due to the accumulation of hydroxyl anions on the adsorbent surface and the increase in the number of negative charges. Due to the fact that fluoride ions are also anionic in nature, the result is thought to be that the removal efficiency is reduced due to the similarity of the surface charges. As(III), on the other hand, is mostly present in its non-ionic form as arsenious acid up to pH 9.2, and, therefore, the effect of pH on As(III) removal is less pronounced than that on the fluoride anions. Furthermore, it was observed (Figure 6) that, as the pH value further increases at more basic values (pH > 7.0), the overall negative value also increases, and there is a drop in the efficiency of the adsorbent, especially in the case of fluoride (Figure 6b), maybe because of the deprotonation, leading to a repulsion of fluoride and As(III) ions and a competition among all three OH⁻, F⁻ and As(III) ions. Therefore, at neutral pH, the removal of anions was achieved through OH⁻ groups, where the surface is neither protonated nor deprotonated [21,25].

Consequently, pH 7 is selected as the optimum value for the simultaneous removal of As(III) and F ions and thus will be used in further experiments to evaluate the adsorption process.

3.2.3. Effect of Initial Concentration

The effect of the initial concentration was studied for both As(III) and F ions in order to evaluate the adsorption on the GO-MnO₂ in the presence of different concentrations of one ion while keeping the other one at constant concentration. Therefore, two different sets of experiments were conducted; in the first one (Figure 8a), the effect of the concentration of F ions (varying from 2–100 mg/L) on As(III) removal (with an initial constant concentration 100 µg/L) was studied, and, in the second one (Figure 8b), the effect of the As(III) concentration (varying from 25–500 µg/L) on F ions removal (with an initial constant concentration 10 mg/L) was studied to evaluate the performance of the GO-MnO₂ in the presence of both ions, at pH 7.0 ± 0.1 , after the application of 2 g/L of the adsorbent at room temperature (298 K).

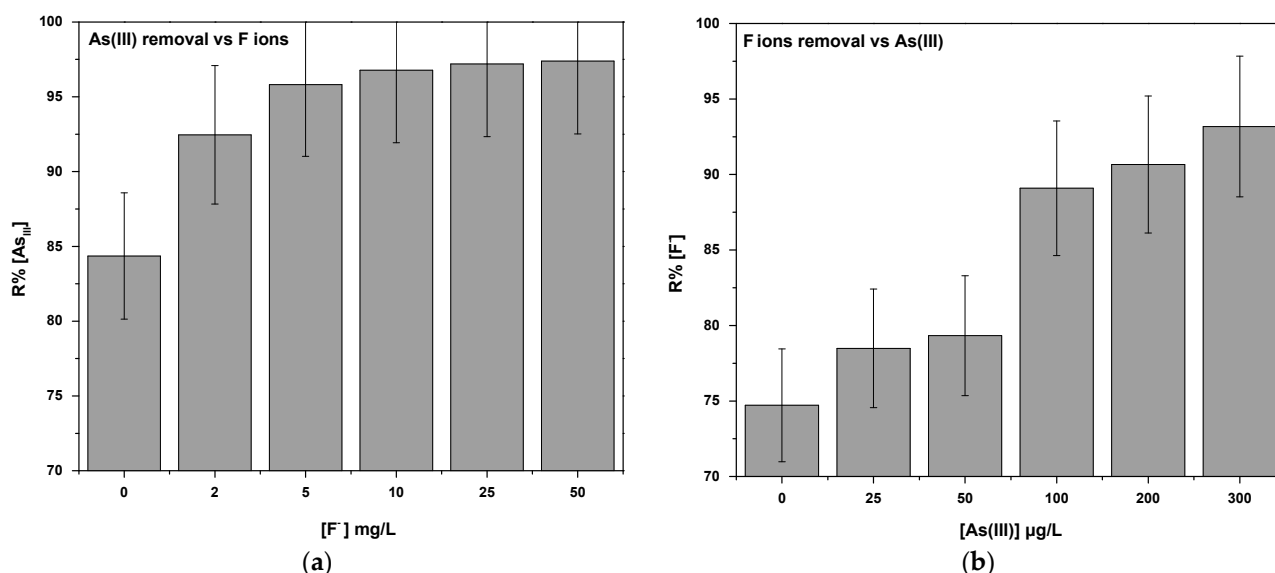


Figure 8. Effect of (a) initial F ions concentration on As(III) R% removal; initial As(III) concentration 100 µg/L; initial F ions concentration 2–100 mg/L; (b) initial As(III) concentration on F ions R% removal; initial As(III) concentration 25–500 µg/L; initial F ions concentration 10 mg/L, pH 7.0 ± 0.1 , dosage 2 g/L, T = 298 K, contact time 24 h, in deionized water.

As depicted in Figure 8a, the percentage removal of As(III) increased impressively from 84 (absence of F ions) to 98% in the presence of F⁻ (100 mg/L). What should be pointed out is that, while, in the absence of fluoride ions, the residual concentration of As(III) was 14.5 µg/L (>10 µg/L), in the presence of even 2 mg/L of fluoride, the residual concentration decreases below the permissible limits (i.e., 6.75 µg/L; 92.5%). Similar achievements were recorded in the second set of experiments, as seen in Figure 8b, where the removal of fluoride ions increases from 74.7% (residual F ions concentration 2.6 mg/L) in the absence of arsenic to 94.3% (residual F ions concentration 0.57 mg/L) in the presence of 500 µg/L of arsenic. It should be noted that a simultaneous As(III) removal took place, indicatively reporting that, when 500 µg/L of arsenic was initially used, its removal was about 89%. Similar behavior was also observed in the recent literature [25].

Consequently, it has been found that both As(III) and fluoride ions can be successfully removed under these experimental conditions, up to the WHO permissible limits (i.e., for F ions 0.6–1.5 mg/L and for As(III) <10 µg/L/L) [2]. This shows the synergic behavior of both ions with GO-MnO₂, and this is in accordance with Figure 3 and the FTIR spectra from which it is concluded that the carboxyl groups of GO-MnO₂ bind both the As(III) and the F⁻ ions, the epoxy groups bind the F ions and the alkoxy groups bind the As(III) ions. Thus, it could be assumed, for the simultaneous presence of the two anions, that initially there is a competition between the As(III) and F ions for covering the carboxyl groups of GO-MnO₂, and possibly that is why the removal rate increases as the feed of one ion increases. Then, as As(III) and F ions are bound in different positions (epoxy groups for F ions, and alkoxy groups for As(III)), a simultaneous removal of the other ion, whose initial concentration is changed, is observed.

This material (GO-MnO₂) is considered as having a very feasible process for up-scaling, especially for small water treatment systems, i.e., at a household level, for areas where the population does not have access to a community drinking water distribution system.

3.2.4. Effect of Contact Time

As contact time is an important parameter for the evaluation of the adsorption, the time required for the adsorbents to reach adsorption equilibrium was determined for the adsorption of As(III) in the presence of F⁻ (Figure 9a) and of F⁻ in the presence of As(III) (Figure 9b). In order to investigate the effect of the contact time, adsorption experiments were performed at an initial As(III) concentration of 100 µg/L and an initial concentration of F ions of 10 mg/L at pH 7.0 ± 0.1, and involved the application of 2 g/L of the adsorbent at room temperature (298 K).

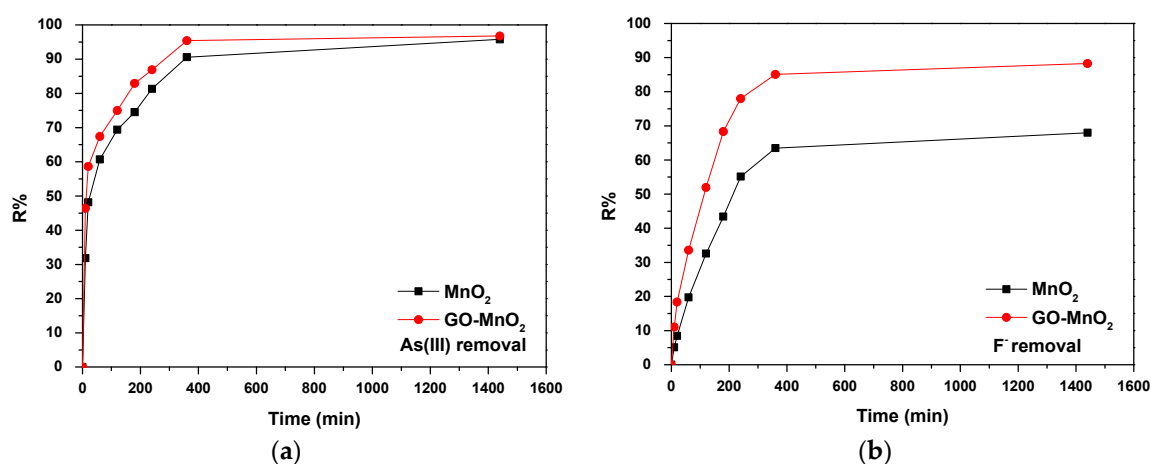


Figure 9. Effect of contact time on the adsorption of (a) As(III) in the presence of F ions, (b) F⁻ in the presence of As(III), in terms of R% removal; initial As(III) concentration 100 µg/L; initial F ions concentration 10 mg/L, pH 7.0 ± 0.1, dosage 2 g/L, T = 298 K, in deionized water.

As shown in Figure 9, the removal of As(III) in the presence of F^- is faster than the removal of F ions in the presence of As(III), as reaching the 50% removal point required only 10 min for As(III), but 120 min for F ions after the application of GO-MnO₂, after which they continued to be adsorbed at a relatively slower rate. In comparison, for the application of MnO₂, the relative required time was higher (i.e., 25 and 200 min for As(III) and F ions, respectively). In both cases, it is observed that the equilibrium is reached after 360 min, after which the percentage of As(III) and F ions removed does not experience much improvement despite the longer contact time.

3.3. Adsorption Isotherms

In order to study the mechanism of adsorption and explain the correlation between the concentration of As(III) and F ions and the adsorption capacity of the adsorbent GO-MnO₂, tests of several adsorption isotherms models were conducted. Specifically, the Langmuir and Freundlich isotherm models were applied in two different sets of experiments. Thus, Figure 10 provides the results for the As(III) removal capacity with the initial concentration varying from 25–500 $\mu\text{g/L}$, in the presence of 10 mg/L of F ions. The relative results for the F ions removal capacity (initial concentration between 2–100 mg/L) in the presence of 100 $\mu\text{g/L}$ of As(III) are presented in Figure 11. The resulting parameters are shown in Tables 2 and 3 for the two models at $\text{pH } 7.0 \pm 0.1$, following an application of 2 g/L of the adsorbent at room temperature (298 K).

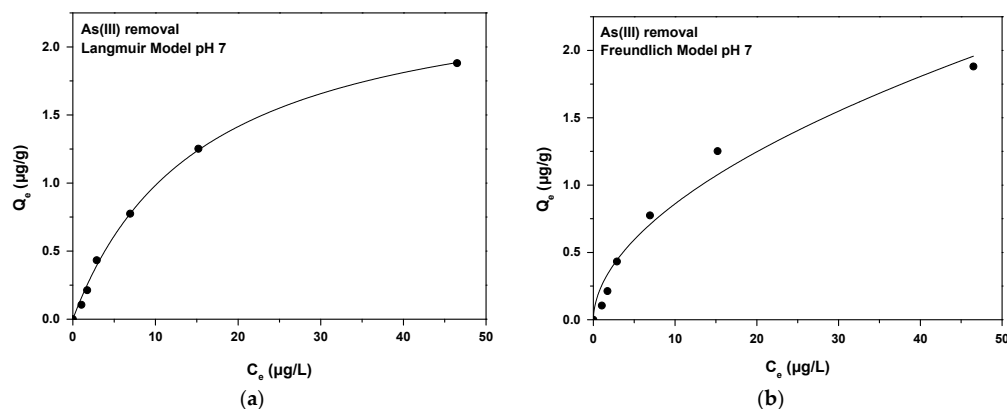


Figure 10. (a) Langmuir and (b) Freundlich isotherm models for the adsorption of As(III) in the presence of F ions; initial As(III) concentration 25–500 $\mu\text{g/L}$; initial F ions concentration 10 mg/L, $\text{pH } 7.0 \pm 0.1$, dosage 2 g/L, $T = 298 \text{ K}$, contact time 24 h, in deionized water.

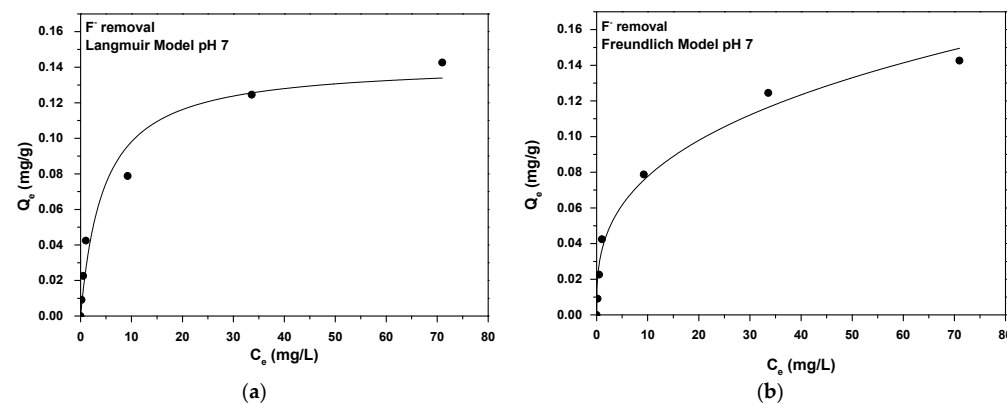


Figure 11. (a) Langmuir and (b) Freundlich isotherm models for the adsorption of F ions in the presence of As(III); initial As(III) concentration 100 $\mu\text{g/L}$; initial F ions concentration 2–100 mg/L, $\text{pH } 7.0 \pm 0.1$, dosage 2 g/L, $T = 298 \text{ K}$, contact time 24 h, in deionized water.

Table 2. Constants of Langmuir and Freundlich isotherm model for the adsorption of As(III) in the presence of F⁻.

Langmuir Isotherm Model				
Adsorbent	Q _m (μg/g)		K _L (L/g)	R ²
GO-MnO ₂	2.52		0.0641	0.9975
Freundlich isotherm model				
Adsorbent	1/n	n	K _F (μg/g)(L/μg) ^{1/n}	R ²
GO-MnO ₂	0.5343	1.8716	0.2516	0.9665

Table 3. Constants of Langmuir and Freundlich isotherm model for the adsorption of F ions in the presence of As(III).

Langmuir Isotherm Model				
Adsorbent	Q _m (mg/g)		K _L (L/g)	R ²
GO-MnO ₂	0.142		0.2208	0.9561
Freundlich isotherm model				
Adsorbent	1/n	n	K _F (mg/g)(L/mg) ^{1/n}	R ²
GO-MnO ₂	0.3344	2.9900	0.0359	0.9804

The Langmuir model assumes that a fixed number of adsorption sites are available on the surface of the adsorbent and can take up one molecule only (monolayer adsorption). On the other hand, the Freundlich model assumes that there are different active sites on the adsorbent surface that have different affinities for different adsorbates (multilayer adsorption). Thus, the adsorption takes place on heterogeneous surfaces. As depicted by the relative parameters (Tables 2 and 3), the Langmuir isotherm model was found to better fit the adsorption of As(III) in the presence of F ions than the Freundlich isotherm model, with a relatively higher correlation coefficient ($R^2 = 0.998$), indicating that As(III) was adsorbed onto the surface of the GO-MnO₂ as a homogeneous monolayer [65]. The maximum theoretical adsorption capacity for As(III) was found to be 2.52 μg/L.

In addition, for F ions removal in the presence of As(III), the Freundlich isotherm model was found to better fit the results ($R^2 = 0.980$). As described earlier in Section 2, for Freundlich model, values of 1/n in the range $0 < 1/n < 1$ assumes that adsorption is favorable. Based on the results shown in Figure 11b and Table 3, the value of 1/n equal to 0.33 for F ions removal in the presence of As(III) suggests that the adsorbent GO-MnO₂ is effective and the adsorption process can be characterized as favorable and heterogeneous and as chemisorption [59].

Based on these assumptions, it follows that the combined removal of As(III) and fluoride ions from aqueous solutions is achieved by different adsorption mechanisms for the two anions.

3.4. Adsorption Kinetics

The pseudo-first order and pseudo-second order models were applied to describe the adsorption of the simultaneous removal of As(III) and fluoride ions on GO-MnO₂. However, the pseudo-first order model did not correlate sufficiently to the obtained results (data not presented). Hence, the experimental data were described with the pseudo-second order model, from which a better correlation was obtained.

Figure 12 presents the PSO kinetic model for the adsorption of As(III) in the presence of F ions (Figure 12a) and of F ions in the presence of As(III) (Figure 12b). The initial As(III) concentration was 100 μg/L, and that of the F ions was 10 mg/L at pH 7.0 ± 0.1 , before

the application of 2 g/L of the adsorbent at room temperature (298 K). The PSO model constants for the application of GO-MnO₂ (calculated from (Equation (6)) are given in Table 4. As shown, the R² for both removal studies is >0.98, indicating that the adsorption fitted excellently to this model. The fitting results led to the conclusion that the adsorption of As(III) in the presence of F ions and of F ions in the presence of As(III) on GO-MnO₂ was closer to chemisorption, and, hence, that there is an exchange or sharing of electrons between the adsorbate and the adsorbent [66,67].

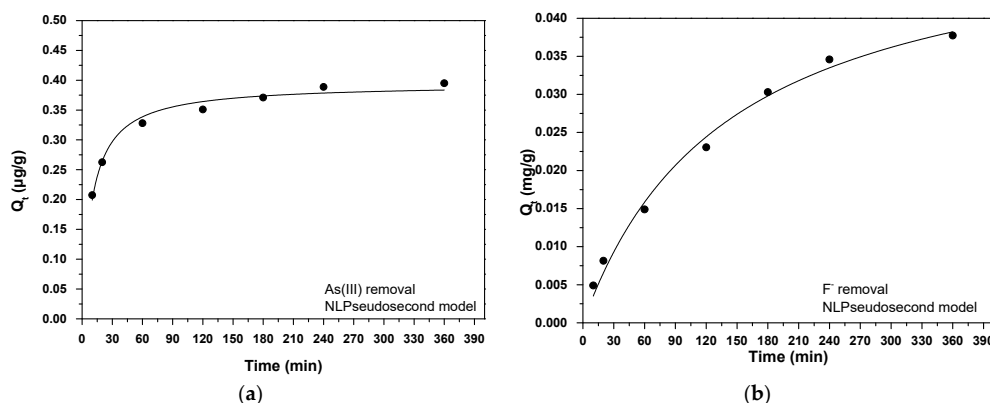


Figure 12. Pseudo-second order kinetic model for the adsorption of (a) As(III) in the presence of F ions; (b) F ions in the presence of As(III); initial As(III) concentration 100 µg/L; initial F ions concentration 10 mg/L, pH 7.0 ± 0.1, dosage 2 g/L, T = 298 K, in deionized water.

Table 4. Pseudo-second order kinetic parameters model for the adsorption of As(III) in the presence of F ions and F ions in the presence of As(III).

Pseudo-Second Order Model (PSO)				
Adsorbent	Q _{e,exp} (µg/g)	K ₂ (L/µg·min)	Q _{e,cal} (µg/g)	R ²
As(III) in presence of F ⁻				
GO-MnO ₂	0.4331	0.2593	0.3939	0.9907
Adsorbent	Q _{e,exp} (mg/g)	K ₂ (L/mg·min)	Q _{e,cal} (mg/g)	R ²
F ⁻ in presence of As(III)				
GO-MnO ₂	0.0392	0.1325	0.0533	0.9895

3.5. Regeneration Study

Regeneration studies were applied in order to examine the reusability of GO-MnO₂ for the simultaneous removal of As(III) and F ions, and the results are shown in Figure 13. After the first cycle, the GO-MnO₂ particles were treated with 0.01 M of NaOH and shaken for 24 h, and then rinsed with distilled water several times in order to remove the excess base amount. A tolerable repetitive time was selected in all applied cycles. As shown in Figure 13, the desorbed adsorbent was tested for up to four repeated cycles for the sorption of As(III) and F ions. In the first cycle, the percentage removal of As(III) was about 96.8%, and, after the fourth, cycle it was about 65.6%. The relative percentage removal of F ions was 88.3 (1st cycle) and 28.7 (4th cycle), respectively.

Consequently, this study confirmed the reuse of the GO-MnO₂ adsorbent for four cycles for As(III) removal (in the presence of F ions), and for three cycles for F ions (in the presence of As(III)) after being successfully regenerated using NaOH treatment. Therefore, three cycles are considered sufficient for the simultaneous removal of As(III) and F ions from water, providing a 20% reduction in the effectiveness of the GO-MnO₂.

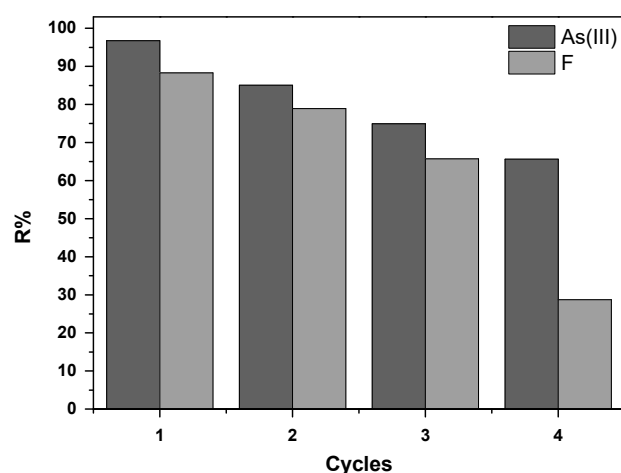


Figure 13. As(III) (in the presence of F ions) and F ions (in the presence of As(III)) adsorption for four adsorption–desorption cycles after regeneration, on GO-MnO₂; initial As(III) concentration 100 µg/L; initial F ions concentration 10 mg/L, pH 7.0 ± 0.1, dosage 2 g/L, T = 298 K, at alkalic pH values, by using 1M NaOH treatment.

4. Conclusions

In this study, the effectiveness of manganese oxide supported on graphene nanostructures (GO-MnO₂) was evaluated for the combined removal of arsenic and fluoride from water. The effect of pH value, initial As(III) and F ions concentration and the dose of the adsorbent were investigated through batch experiments, while the structure and the morphology of GO-MnO₂ were analyzed using EDS, FTIR and SEM.

The results showed that a dose of 2 g/L of GO-MnO₂ at neutral pH conditions could decrease the As(III) and F ion concentrations simultaneously to the desired values according to the permissible WHO limits. Consequently, it has been found that the percentage removal of As(III) increased impressively from 84 (in the absence of F ions) to 98% in the presence of F ions (100 mg/L), while the removal of fluoride ions increased from 74.7% (a residual F ions concentration of 2.6 mg/L) in the absence of arsenic to 94.3% (a residual F ions concentration of 0.57 mg/L) in the presence of 500 µg/L of arsenic. Thus, it has been found that both As(III) and fluoride ions can be successfully removed under these experimental conditions, to concentrations below the WHO permissible limits (i.e., for F ions 0.6–1.5 mg/L and for As(III) <10 µg/L). This shows the synergic behavior of both ions with GO-MnO₂, which was also explained by the FTIR spectra.

The Langmuir isotherm model was found to better fit the adsorption of As(III) in the presence of F[−] ($R^2 = 0.998$), and the Freundlich isotherm model was found to better fit the adsorption of F[−] in the presence of As(III) ($R^2 = 0.980$), indicating that As(III) was adsorbed onto the surface of the GO-MnO₂ as a homogeneous monolayer, while the adsorption process of F ions can be characterized as favorable and heterogeneous and as chemisorption.

Moreover, the experimental data were described better with the pseudo-second order model, from which a better correlation was obtained, leading to the conclusion that the adsorption of As(III) in the presence of F ions and of F ions in the presence of As(III) on GO-MnO₂ was closer to chemisorption, and, hence, that there is an exchanging or sharing of electrons between the adsorbate and the adsorbent.

Finally, regeneration studies were conducted using 0.01 M of NaOH, and it was shown that three cycles are considered sufficient for the simultaneous removal of As(III) and F ions from water, providing a 20% reduction in the effectiveness of GO-MnO₂.

Author Contributions: Conceptualization, A.K.T., I.A.K., G.Z.K. and E.A.D.; methodology, A.K.T., I.A.K., G.Z.K., E.A.D. and D.G.T.; validation, A.K.T., I.A.K., G.Z.K. and E.A.D.; formal analysis, A.K.T., D.G.T., I.A.K., G.Z.K. and E.A.D.; investigation, A.K.T., S.T, G.Z.K. and I.A.K.; resources, A.K.T.,

D.G.T., I.A.K., G.Z.K. and E.A.D.; data curation, A.K.T. and D.G.T.; writing—original draft preparation, A.K.T.; writing—review and editing, A.K.T., D.G.T., I.A.K., G.Z.K. and E.A.D.; visualization, A.K.T., D.G.T., I.A.K., G.Z.K. and E.A.D.; supervision, A.K.T., I.A.K., G.Z.K. and E.A.D. All authors have read and agreed to the published version of the manuscript.

Funding: Support for this study was received from the Prefecture of Central Macedonia in Greece, under the framework of the research project “Selection of research directions and accreditation of parameters and methods of the chemical and biological sector of the Laboratory of Environmental Control and Research of Prefecture of Central Macedonia,” with the ID number 71658 at the research committee of Aristotle University of Thessaloniki.

Institutional Review Board Statement: Not applicable.

Informed Consent Statement: Not applicable.

Data Availability Statement: The data presented in this study are available upon request, from the corresponding author.

Conflicts of Interest: The authors declare no conflict of interest.

References

1. Chouhan, S.; Flora, S.J.S. Arsenic and fluoride: Two major ground water pollutants. *Indian J. Exp. Biol.* **2010**, *48*, 666–678. [[PubMed](#)]
2. World Health Organization. World Health Organization European Standards for Drinking-Water. *Am. J. Med. Sci.* **1970**, *242*, 56.
3. Smith, A.H.; Steinmaus, C.M. Health effects of arsenic and chromium in drinking water: Recent human findings. *Annu. Rev. Public Health* **2009**, *30*, 107–122. [[CrossRef](#)] [[PubMed](#)]
4. Trikkaliotis, D.G.; Ainali, N.M.; Tolkou, A.K.; Mitropoulos, A.C.; Lambropoulou, D.A.; Bikiaris, D.N.; Kyzas, G.Z. Removal of Heavy Metal Ions from Wastewaters by Using Chitosan/Poly(Vinyl Alcohol) Adsorbents: A Review. *Macromol* **2022**, *2*, 26. [[CrossRef](#)]
5. Arya, S.; Subramani, T.; Vennila, G.; Karunanidhi, D. Health risks associated with fluoride intake from rural drinking water supply and inverse mass balance modeling to decipher hydrogeochemical processes in Vattamalaikarai River basin, South India. *Environ. Geochem. Health* **2019**, *43*, 705–716. [[CrossRef](#)] [[PubMed](#)]
6. Alarcón-Herrera, M.T.; Martín-Alarcon, D.A.; Gutiérrez, M.; Reynoso-Cuevas, L.; Martín-Domínguez, A.; Olmos-Márquez, M.A.; Bundschuh, J. Co-occurrence, possible origin, and health-risk assessment of arsenic and fluoride in drinking water sources in Mexico: Geographical data visualization. *Sci. Total Environ.* **2020**, *698*, 134168. [[CrossRef](#)]
7. Katsoyiannis, I.A.; Zouboulis, A.I. Comparative evaluation of conventional and alternative methods for the removal of arsenic from contaminated groundwaters. *Rev. Environ. Health* **2006**, *21*, 25–41. [[CrossRef](#)]
8. Katsoyiannis, I.A.; Voegelin, A.; Zouboulis, A.I.; Hug, S.J. Enhanced As(III) oxidation and removal by combined use of zero valent iron and hydrogen peroxide in aerated waters at neutral pH values. *J. Hazard. Mater.* **2015**, *297*, 1–7. [[CrossRef](#)] [[PubMed](#)]
9. Cullen, W.R.; Reimer, K.J. Arsenic Speciation in the Environment. *Chem. Rev.* **1989**, *89*, 713–764. [[CrossRef](#)]
10. Aposhian, H.V.; Zakharyan, R.A.; Avram, M.D.; Kopplin, M.J.; Wollenberg, M.L. Oxidation and detoxification of trivalent arsenic species. *Toxicol. Appl. Pharmacol.* **2003**, *193*, 1–8. [[CrossRef](#)]
11. Farooqi, A.; Masuda, H.; Firdous, N. Toxic fluoride and arsenic contaminated groundwater in the Lahore and Kasur districts, Punjab, Pakistan and possible contaminant sources. *Environ. Pollut.* **2007**, *145*, 839–849. [[CrossRef](#)]
12. Ingallinella, A.M.; Pacini, V.A.; Fernández, R.G.; Vidoni, R.M.; Sanguinetti, G. Simultaneous removal of arsenic and fluoride from groundwater by coagulation-adsorption with polyaluminum chloride. *J. Environ. Sci. Health-Part A Toxic/Hazardous Subst. Environ. Eng.* **2011**, *46*, 1288–1296. [[CrossRef](#)] [[PubMed](#)]
13. López-Guzmán, M.; Alarcón-Herrera, M.T.; Irigoyen-Campuzano, J.R.; Torres-Castañón, L.A.; Reynoso-Cuevas, L. Simultaneous removal of fluoride and arsenic from well water by electrocoagulation. *Sci. Total Environ.* **2019**, *678*, 181–187. [[CrossRef](#)] [[PubMed](#)]
14. Tolkou, A.K.; Meez, E.; Kyzas, G.Z.; Torretta, V.; Collivignarelli, M.C.; Caccamo, F.M.; Deliyanni, E.A.; Katsoyiannis, I.A. A Mini Review of Recent Findings in Cellulose-, Polymer- and Drinking Water. *C—Journal Carbon Res.* **2021**, *7*, 74. [[CrossRef](#)]
15. Tolkou, A.K.; Manousi, N.; Zachariadis, G.A.; Katsoyiannis, I.A.; Deliyanni, E.A. Recently developed adsorbing materials for fluoride removal from water and fluoride analytical determination techniques: A review. *Sustainability* **2021**, *13*, 7061. [[CrossRef](#)]
16. Laskaridis, A.; Sarakatsianos, I.; Tzollas, N.; Katsoyiannis, I.A. Simultaneous removal of arsenate and chromate from ground- and surface- waters by iron-based redox assisted coagulation. *Sustainability* **2020**, *12*, 5394. [[CrossRef](#)]
17. Qiao, J.; Cui, Z.; Sun, Y.; Hu, Q.; Guan, X. Simultaneous removal of arsenate and fluoride from water by Al-Fe (hydr)oxides. *Front. Environ. Sci. Eng.* **2014**, *8*, 169–179. [[CrossRef](#)]
18. Tolkou, A.K.; Kyzas, G.Z.; Katsoyiannis, I.A. Arsenic(III) and Arsenic(V) Removal from Water Sources by Molecularly Imprinted Polymers (MIPs): A Mini Review of Recent Developments. *Sustainability* **2022**, *14*, 5222. [[CrossRef](#)]

19. Luo, X.; Lei, X.; Cai, N.; Xie, X.; Xue, Y.; Yu, F. Removal of heavy metal ions from water by magnetic cellulose-based beads with embedded chemically modified magnetite nanoparticles and activated carbon. *ACS Sustain. Chem. Eng.* **2016**, *4*, 3960–3969. [[CrossRef](#)]
20. Rahaman, M.; Das, A.; Bose, S. Development of copper—Iron bimetallic nanoparticle impregnated activated carbon derived from coconut husk and its efficacy as a novel adsorbent toward the removal of chromium (VI) from aqueous solution. *Water Environ. Res.* **2021**, *93*, 1417–1427. [[CrossRef](#)]
21. Kyzas, G.Z.; Tolkou, A.K.; Al Musawi, T.J.; Mengelizadeh, N.; Mohebi, S.; Balarak, D. Fluoride Removal from Water by Using Green Magnetic Activated Carbon Derived from Canola Stalks. *Water Air Soil Pollut.* **2022**, *233*, 424. [[CrossRef](#)]
22. Meez, E.; Tolkou, A.K.; Giannakoudakis, D.A.; Katsoyiannis, I.A.; Kyzas, G.Z. Activated Carbons for Arsenic Removal from Natural Waters and Wastewaters: A Review. *Water* **2021**, *13*, 2982. [[CrossRef](#)]
23. Bibi, S.; Farooqi, A.; Hussain, K.; Haider, N. Evaluation of industrial based adsorbents for simultaneous removal of arsenic and fluoride from drinking water. *J. Clean. Prod.* **2015**, *87*, 882–896. [[CrossRef](#)]
24. Jadhav, S.V.; Bringas, E.; Yadav, G.D.; Rathod, V.K.; Ortiz, I.; Marathe, K.V. Arsenic and fluoride contaminated groundwaters: A review of current technologies for contaminants removal. *J. Environ. Manage* **2015**, *162*, 306–325. [[CrossRef](#)] [[PubMed](#)]
25. Gupta, A.R.; Joshi, V.C.; Yadav, A.; Sharma, S. Synchronous Removal of Arsenic and Fluoride from Aqueous Solution: A Facile Approach to Fabricate Novel Functional Metallopolymer Microspheres. *ACS Omega* **2022**, *7*, 4879–4891. [[CrossRef](#)]
26. Xi, B.; Wang, X.; Liu, W.; Xia, X.; Li, D.; He, L.; Wang, H.; Sun, W.; Yang, T.; Tao, W. Fluoride and Arsenic Removal by Nanofiltration Technology from Groundwater in Rural Areas of China: Performances with Membrane Optimization. *Sep. Sci. Technol.* **2014**, *49*, 2642–2649. [[CrossRef](#)]
27. Thakur, L.S.; Goyal, H.; Mondal, P. Simultaneous removal of arsenic and fluoride from synthetic solution through continuous electrocoagulation: Operating cost and sludge utilization. *J. Environ. Chem. Eng.* **2019**, *7*, 102829. [[CrossRef](#)]
28. Murthy, S.; Shivaswamy, M.; Mahesh, S.; Hanumanthappa, S. Simultaneous Removal of Arsenite and Fluoride from Groundwater using Batch Electrochemical Coagulation Process-Role of Aluminum with Iron Electrodes. *Orient. J. Chem.* **2019**, *35*, 85–97. [[CrossRef](#)]
29. Tolkou, A.K.; Katsoyiannis, I.A.; Zouboulis, A.I. Removal of arsenic, chromium and uranium from water sources by novel nanostructured materials including graphene-based modified adsorbents: A mini review of recent developments. *Appl. Sci.* **2020**, *10*, 3241. [[CrossRef](#)]
30. García-Chirino, J.; Mercado-Borrayo, B.M.; Schouwenaars, R.; González-Chávez, J.L.; Ramírez-Zamora, R.M. Simultaneous removal of arsenic and fluoride from water using iron and steel slags. In *Environmental Arsenic in a Changing World*; CRC Press: Boca Raton, FL, USA, 2019; pp. 580–581. [[CrossRef](#)]
31. Chunhui, L.; Jin, T.; Puli, Z.; Bin, Z.; Duo, B.; Xuebin, L. Simultaneous removal of fluoride and arsenic in geothermal water in Tibet using modified yak dung biochar as an adsorbent. *R. Soc. Open Sci.* **2018**, *5*, 181266. [[CrossRef](#)]
32. Yan, L.; Tu, H.; Chan, T.; Jing, C. Mechanistic study of simultaneous arsenic and fluoride removal using granular TiO₂-La adsorbent. *Chem. Eng. J.* **2017**, *313*, 983–992. [[CrossRef](#)]
33. Hou, T.; Kong, L.; Guo, X.; Wu, Y.; Wang, F.; Wen, Y.; Yang, H. Magnetic ferrous-doped graphene for improving Cr (VI) removal. *Mater. Res. Express* **2016**, *3*, 045006. [[CrossRef](#)]
34. Yu, J.G.; Yu, L.Y.; Yang, H.; Liu, Q.; Chen, X.H.; Jiang, X.Y.; Chen, X.Q.; Jiao, F.P. Graphene nanosheets as novel adsorbents in adsorption, preconcentration and removal of gases, organic compounds and metal ions. *Sci. Total Environ.* **2015**, *502*, 70–79. [[CrossRef](#)]
35. Mishra, T.; Mahato, D.K. A comparative study on enhanced arsenic(V) and arsenic(III) removal by iron oxide and manganese oxide pillared clays from ground water. *J. Environ. Chem. Eng.* **2016**, *4*, 1224–1230. [[CrossRef](#)]
36. Rath, B.; Jamieson, J.; Sun, J.; Siade, A.J.; Zhu, M.; Cirpka, O.A.; Prommer, H. Process-based modeling of arsenic(III) oxidation by manganese oxides under circumneutral pH conditions. *Water Res.* **2020**, *185*, 116195. [[CrossRef](#)]
37. Sivasankar, V.; Ramachandramoorthy, T.; Darchen, A. Manganese dioxide improves the efficiency of earthenware in fluoride removal from drinking water. *Desalination* **2011**, *272*, 179–186. [[CrossRef](#)]
38. Zhao, J.; Liu, J.; Li, N.; Wang, W.; Nan, J.; Zhao, Z.; Cui, F. Highly efficient removal of bivalent heavy metals from aqueous systems by magnetic porous Fe₃O₄-MnO₂: Adsorption behavior and process study. *Chem. Eng. J.* **2016**, *304*, 737–746. [[CrossRef](#)]
39. He, C.; Xie, F. Adsorption Behavior of Manganese Dioxide Towards Heavy Metal Ions: Surface Zeta Potential Effect. *Water. Air. Soil Pollut.* **2018**, *229*, 77. [[CrossRef](#)]
40. Dong, L.; Zhu, Z.; Ma, H.; Qiu, Y.; Zhao, J. Simultaneous adsorption of lead and cadmium on MnO₂-loaded resin. *J. Environ. Sci.* **2010**, *22*, 225–229. [[CrossRef](#)] [[PubMed](#)]
41. Zhang, H.; Xu, F.; Xue, J.; Chen, S.; Wang, J.; Yang, Y. Enhanced removal of heavy metal ions from aqueous solution using manganese dioxide-loaded biochar: Behavior and mechanism. *Sci. Rep.* **2020**, *10*, 6067. [[CrossRef](#)]
42. Yang, Y.; Wang, Y.; Li, X.; Xue, C.; Dang, Z.; Zhang, L.; Yi, X. Effects of synthesis temperature on ε-MnO₂ microstructures and performance: Selective adsorption of heavy metals and the mechanism onto (100) facet compared with (001). *Environ. Pollut.* **2022**, *315*, 120218. [[CrossRef](#)] [[PubMed](#)]
43. Chen, J.; Dong, R.; Chen, S.; Tang, D.; Lou, X.; Ye, C.; Qiu, T.; Yan, W. Selective adsorption towards heavy metal ions on the green synthesized polythiophene/MnO₂ with a synergetic effect. *J. Clean. Prod.* **2022**, *338*, 130536. [[CrossRef](#)]

44. Luo, X.; Wang, C.; Wang, L.; Deng, F.; Luo, S.; Tu, X.; Au, C. Nanocomposites of graphene oxide-hydrated zirconium oxide for simultaneous removal of As(III) and As(V) from water. *Chem. Eng. J.* **2013**, *220*, 98–106. [CrossRef]
45. Luo, X.; Wang, C.; Luo, S.; Dong, R.; Tu, X.; Zeng, G. Adsorption of As (III) and As (V) from water using magnetite Fe₃O₄-reduced graphite oxide-MnO₂ nanocomposites. *Chem. Eng. J.* **2012**, *187*, 45–52. [CrossRef]
46. Guan, C.; Lv, X.; Han, Z.; Chen, C.; Xu, Z.; Liu, Q. The adsorption enhancement of graphene for fluorine and chlorine from water. *Appl. Surf. Sci.* **2020**, *516*, 146157. [CrossRef]
47. Barathi, M.; Krishna Kumar, A.S.; Kumar, C.U.; Rajesh, N. Graphene oxide-aluminium oxyhydroxide interaction and its application for the effective adsorption of fluoride. *RSC Adv.* **2014**, *4*, 53711–53721. [CrossRef]
48. Prathibha, C.; Biswas, A.; Chunduri, L.A.A.; Reddy, S.K.; Loganathan, P.; Kalaruban, M.; Venkatarmaniah, K. Zr(IV) functionalized graphene oxide anchored sand as potential and economic adsorbent for fluoride removal from water. *Diam. Relat. Mater.* **2020**, *109*, 108081. [CrossRef]
49. Nor, N.M.; Kamil, N.H.N.; Mansor, A.I.; Maarof, H.I. Adsorption Analysis of Fluoride Removal Using Graphene Oxide/Eggshell Adsorbent. *Indones. J. Chem.* **2020**, *20*, 579. [CrossRef]
50. Gao, Y.; You, K.; Fu, J.; Wang, J.; Qian, W. Manganese Modified Activated Alumina through Impregnation for Enhanced Adsorption Capacity of Fluoride Ions. *Water* **2022**, *14*, 2673. [CrossRef]
51. Saroyan, H.; Kyzas, G.Z.; Deliyanni, E.A. Effective dye degradation by graphene oxide supported manganese oxide. *Processes* **2019**, *7*, 40. [CrossRef]
52. He, Y.; Chen, W.; Li, X.; Zhang, Z.; Fu, J.; Zhao, C.; Xie, E. Freestanding three-dimensional graphene/MnO₂ composite networks as ultralight and flexible supercapacitor electrodes. *ACS Nano* **2013**, *7*, 174–182. [CrossRef] [PubMed]
53. Trikkaliotis, D.G.; Christoforidis, A.K.; Mitropoulos, A.C.; Kyzas, G.Z. Graphene oxide synthesis, properties and characterization techniques: A comprehensive review. *ChemEngineering* **2021**, *5*, 64. [CrossRef]
54. Zhang, K.; Dwivedi, V.; Chi, C.; Wu, J. Graphene oxide/ferric hydroxide composites for efficient arsenate removal from drinking water. *J. Hazard. Mater.* **2010**, *182*, 162–168. [CrossRef] [PubMed]
55. Tolkou, A.K.; Zouboulis, A.I. Graphene Oxide/Fe-Based Composite Pre-Polymerized Coagulants: Synthesis, Characterization, and Potential Application in Water Treatment. *C—J. Carbon Res.* **2020**, *6*, 44. [CrossRef]
56. Hummers, W.S.; Offeman, R.E. Preparation of Graphitic Oxide. *J. Am. Chem. Soc.* **1957**, *208*, 1937. [CrossRef]
57. Debnath, S.; Maity, A.; Pillay, K. Impact of process parameters on removal of Congo red by graphene oxide from aqueous solution. *J. Environ. Chem. Eng.* **2014**, *2*, 260–272. [CrossRef]
58. APHA Standard Methods for the Examination of Water and Wastewater. 1981. Available online: https://beta-static.fishersci.com/content/dam/fishersci/en_US/documents/programs/scientific/technical-documents/white-papers/apha-water-testing-standard-methods-introduction-white-paper.pdf (accessed on 5 December 2022).
59. Tolkou, A.K.; Trikalioti, S.; Makrogianni, O.; Katsoyiannis, I.A. Magnesium modified activated carbons derived from coconut shells for the removal of fluoride from water. *Sustain. Chem. Pharm.* **2023**, *31*, 100898. [CrossRef]
60. Swenson, H.; Stadie, N.P. Langmuir's Theory of Adsorption: A Centennial Review. *Langmuir* **2019**, *35*, 5409–5426. [CrossRef]
61. Freundlich, H. Über die Adsorption in Lösungen. *Zeitschrift für Phys. Chemie* **1907**, *57*, 385–470. [CrossRef]
62. Trikkaliotis, D.G.; Mitropoulos, A.C.; Kyzas, G.Z. Low-cost route for top-down synthesis of over- and low-oxidized graphene oxide. *Colloids Surfaces A Physicochem. Eng. Asp.* **2020**, *600*, 124928. [CrossRef]
63. Tran, V.M.; Ha, A.T.; Le, M.L.P. Capacitance behavior of nanostructured ε-MnO₂/C composite electrode using different carbons matrix. *Adv. Nat. Sci. Nanosci. Nanotechnol.* **2014**, *5*, 025005. [CrossRef]
64. Babaeiveli, K.; Khodadoust, A.P. Removal of arsenic from water using manganese (III) oxide: Adsorption of As(III) and As(V). *J. Environ. Sci. Health-Part A Toxic/Hazardous Subst. Environ. Eng.* **2016**, *51*, 277–288. [CrossRef]
65. Hashimi, S.Q.; Hong, S.H.; Lee, C.G.; Park, S.J. Adsorption of Arsenic from Water Using Aluminum-Modified Food Waste Biochar: Optimization Using Response Surface Methodology. *Water* **2022**, *14*, 2712. [CrossRef]
66. Ho, Y.S.; McKay, G. Pseudo-second order model for sorption processes. *Process Biochem.* **1999**, *34*, 451–465. [CrossRef]
67. Jha, M.K.; Joshi, S.; Sharma, R.K.; Kim, A.A.; Pant, B.; Park, M.; Pant, H.R. Surface modified activated carbons: Sustainable bio-based materials for environmental remediation. *Nanomaterials* **2021**, *11*, 3140. [CrossRef] [PubMed]

Disclaimer/Publisher's Note: The statements, opinions and data contained in all publications are solely those of the individual author(s) and contributor(s) and not of MDPI and/or the editor(s). MDPI and/or the editor(s) disclaim responsibility for any injury to people or property resulting from any ideas, methods, instructions or products referred to in the content.